SCIENTIFIC Publishing Limited

New Energy Exploitation and Application

https://ojs.ukscip.com/journals/neea

Article

Direct Absorption Solar Collector: An Experimental Investigation of Al_2O_3-H_2O Nanofluid over the Flat Plate at Different Tilt Angles, and Mass-Flow Rates

Lalit Jyani [1], Shivangi Sharma [2,*], Kailash Chaudhary [1], Kamlesh Purohit [1]

[1] Department of Mechanical Engineering, MBM University, Jodhpur, Rajasthan 342001, India
[2] Birmingham Energy Institute, Department of Chemical Engineering, University of Birmingham, Birmingham B15 2TT, United Kingdom
[*] Correspondence: s.sharma@bham.ac.uk

Received: 30 December 2023; **Revised**: 23 January 2024; **Accepted**: 20 February 2024; **Published**: 29 February 2024

Abstract: The escalating demand for solar thermal energy, coupled with the current inefficiencies in existing systems, underscores the critical need for innovative advancements in thermal storage solar collectors. The efficiency of solar collectors relies not solely on design effectiveness but also on the thermophysical properties, such as heat capacity and thermal conductivity, inherent in the working fluid. This study investigates a novel solar collector with a gross area of 0.36 m^2, operating on the principle of direct absorption. Experimental investigations were done at various tilt angles (15°, 20°, and 30°) with respect to the horizontal, considering different flow rates and nanofluid settlement within the base fluids. The use of Al_2O_3 nanoparticles into the base fluid as water, exhibits significant positive effects on the thermophysical properties of the nanofluids, with a volume concentration of 0.003%. The efficiency of the solar collector was calculated across three mass flow rates (0.5, 1, and 1.33 L/min) at each tilt angle. Notably, the study reveals that the efficiency peaks at a 15° tilt due to an optimal flow configuration for maximum energy harvest across all three mass flow rates. Increasing the mass flow rate yields efficiency increments for all tilt angles (15°, 20°, and 30°), with 1 L/min emerging as the optimal mass-flow rate in most cases. This research not only addresses the immediate need for improved solar thermal technologies but also aligns with global sustainability goals, contributing to the IEA Net Zero Emissions initiative and supporting UN Sustainable Development Goals 7, 9, and 11. The paper also includes a critical literature review on the use of nanofluids in solar thermal collectors to improve thermo-physical properties and enhance solar efficiency. Additionally, the key findings regarding the influence and tilt angle on solar efficiency are discussed.

Keywords: solar thermal collector (STC); direct absorption solar collector (DASC); Al_2O_3-H_2O nanofluid; impact of tilt angle; effects of mass flow rate

1. Introduction

Solar thermal energy is one of the most popular renewable sources of sustainable energy with the least environmental impact, no requirement of transportation, and free availability for every human being all over the world. Solar thermal collectors are widely used systems for the collection and conversion of solar energy into thermal energy or heat [1]. Due to an increase in the demand for solar thermal energy in various fields, there is a pressing requirement for improvements in the design of solar collector systems [2,3] to harvest the maximum

irradiation on the collector surface. In conventional-type thermal solar collectors, the incoming solar rays fall over the absorber plate which absorbs the solar radiation and converts it into heat. This heat is then conducted from the absorber plate to the tubes carrying the fluids and then through convection via the working fluid. Due to the involvement of three transfer mediums between the solar radiations and the working fluid, the losses are more pronounced [4]. To reduce these convection and conduction losses requires minimizing these transfer mediums and there is a need for such a collector which directly transfers solar radiation to working fluid. Direct Absorption Solar Collector is such type of solar collector that directly absorbs solar radiation, reducing the resistance between the source and the working fluid will be studied in detail in the next sections.

The total operational solar thermal capacity reached 522 GW_{th} globally by 2021 with a collection area of 746 million m^2; showing a 21 GW_{th} (31 million m^2) growth within the year [5]. In the global scenario, there were 250 million dwellings in 2020 with solar thermal technologies for water heating application with a target of 400 million to be reached by 2030 as per the IEA Net Zero Emissions by 2050 Scenario. The IEA Solar Heating and Cooling TCP estimates that a hybrid approach will be needed, using the existing technologies based on 170 million new solar thermal systems, and novel technologies based on 120 million installations by 2030 (Figure 1) [6].

The authors of [5] studied the Photovoltaic Thermal (PVT) collectors as a market leading technology in recent years along with the collector types such as unglazed, glazed flat-plate collectors and evacuated tube collectors with water, the glazed and unglazed air collectors through survey of the national delegates. Figure 2 shows the annual installed collector capacities and the net additions in 2021.

Solar thermal collector devices absorb solar radiation and convert it into heat, which is then transferred to commonly used heat transfer fluids (HTF) or a nanofluid. A broad categorisation of the technology is shown in Figure 3 with respect to concentration and operational temperatures. While low-temperature solar thermal collectors (STC) such as unglazed flat plates are generally used to heat swimming pools, the medium-temperature glazed flat-plate and evacuated tube collectors are used for air and water heating applications in buildings [7].

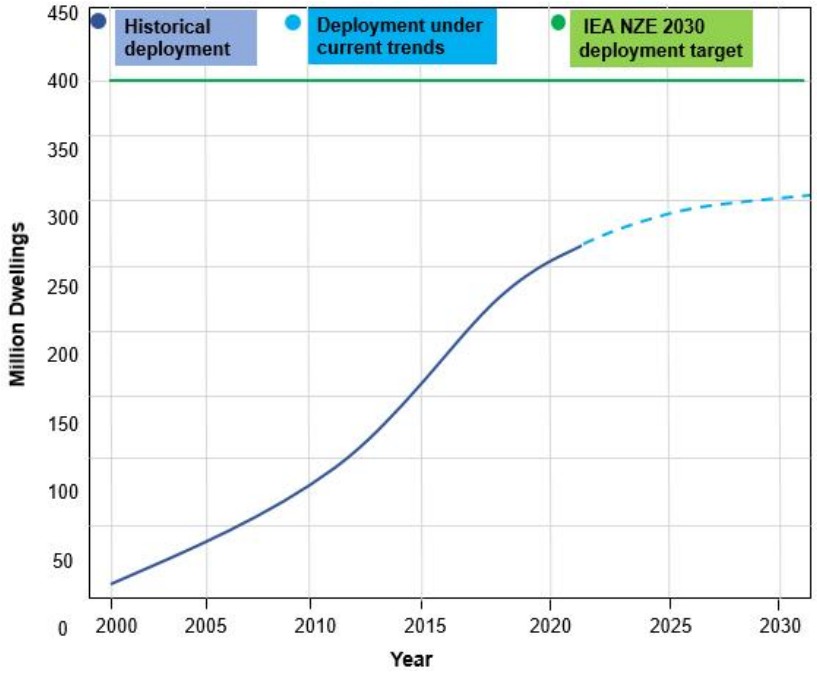

Figure 1. Solar thermal technologies under current trends with respect to the Net Zero scenario deployment target to 2030 (IEA) redrawn using [6].

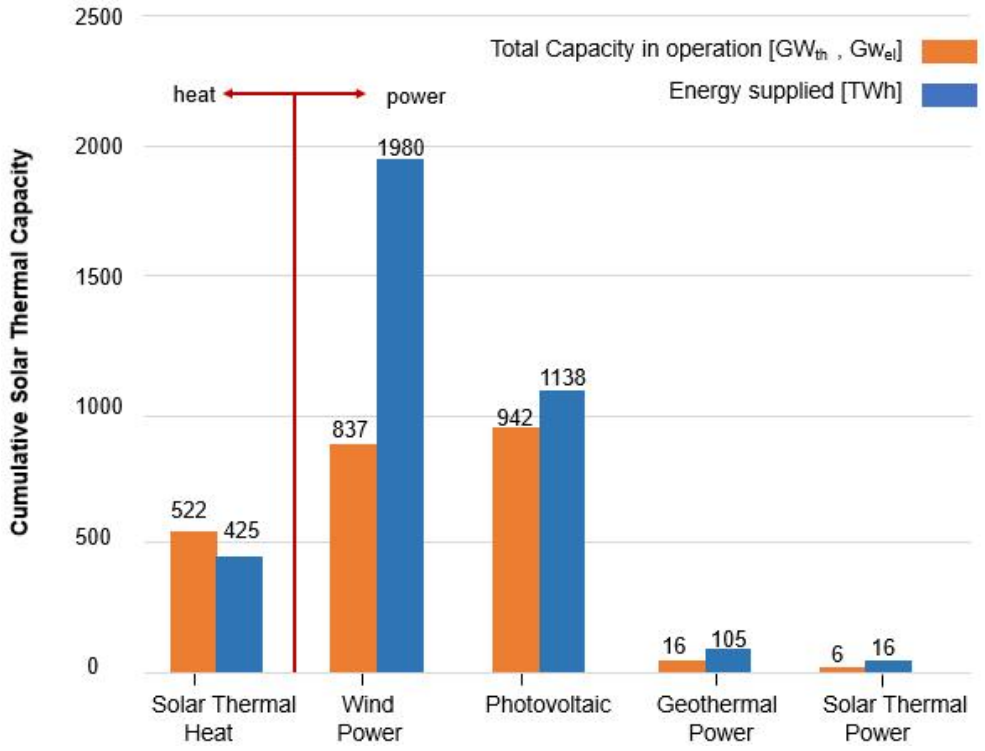

Figure 2. The worldwide total capacity in operation (GW_{el}, GW_{th}) in 2021 and the annual energy (electricity and heat) yields (TWh_{el}, TWh_{th}) [5].

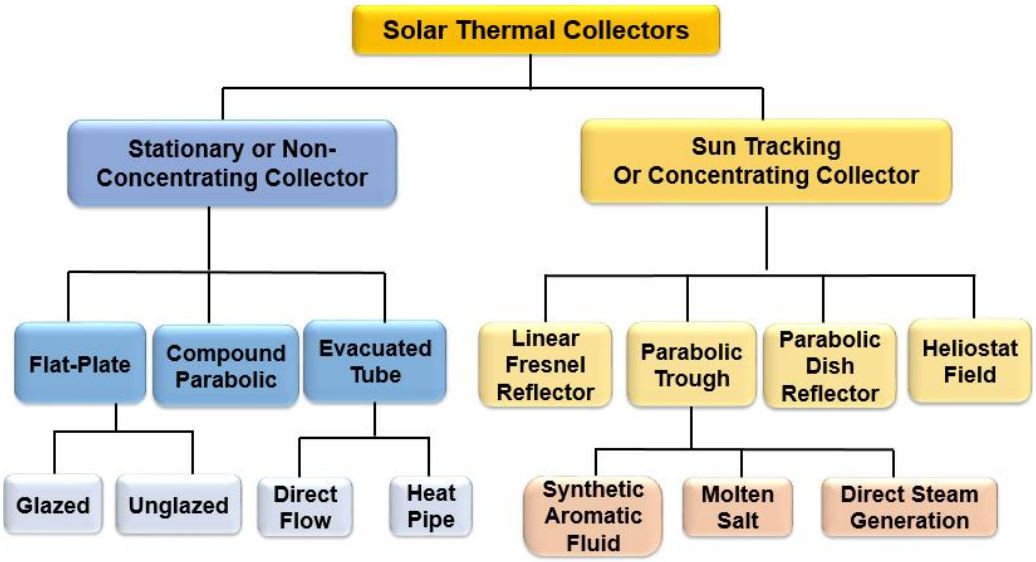

(**a**)

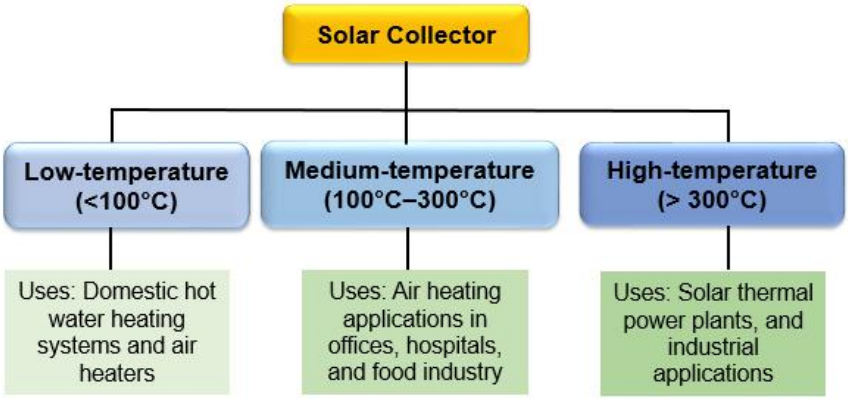

(**b**)

Figure 3. Classification of solar collectors based on (**a**) concentration, and (**b**) temperatures (drawn using references [7,8]).

In order to improve the efficiency of a solar thermal collector, researchers proposed a concept of directly absorbing the solar energy within the fluid volume in the 1970s called Direct Absorption Solar Collector (DASC) [9]. In a DASC, the HTF absorbs incident radiation volumetrically, as a result of which more homogeneous temperature distribution and reduced heat losses are experienced than in the conventional surface collectors (Figure 4) [10].

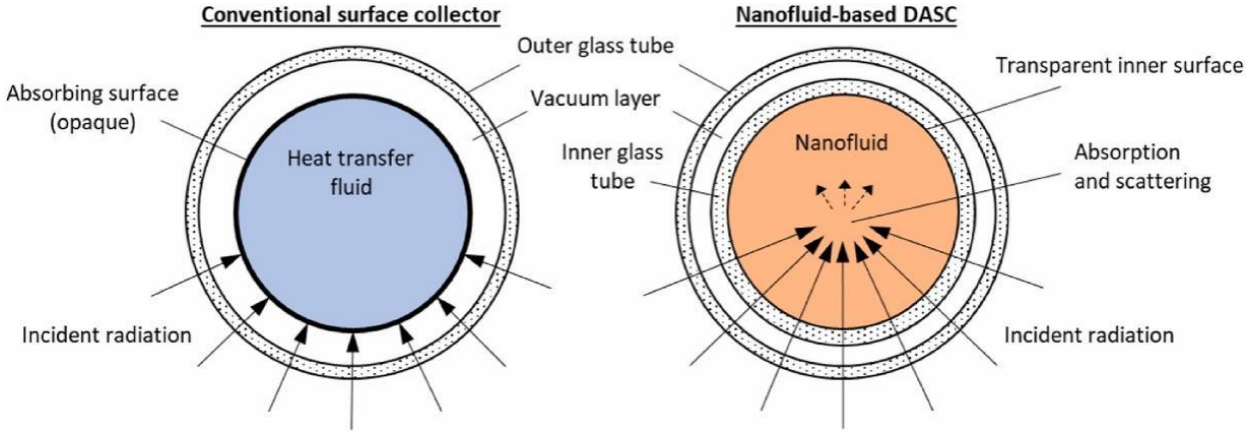

Figure 4. A schematic of the difference in the optical principle of a conventional tubular surface collector versus a nanofluid-based tubular DASC [10].

However, the efficiency of direct absorption collector is limited by the absorption properties of the conventional working fluid, which is very poor over the range of the wavelength in the solar spectrum [11]. In the beginning, black liquids containing millimetre to micrometre sized particles were used as a working fluid in the DASCs to enhance the absorption of solar radiation which led to efficiency improvements. The applications of micron-sized particles into the base fluid for DASCs lead to pipe blockage, erosion, abrasion and poor stability. Particle sedimentation from the suspensions results in clogged channels [12]. In a DASC, nanoparticles are added to a base fluid to form nanofluids as an HTF [12]. Upon adding nanoparticles in the base fluid due to Brownian movement, the thermophysical property of the fluid is enhanced. Particle migration can have great influences on the characteristics of nanofluids by disturbing the distribution of nanoparticle concentration and thermophysical properties. Flow-induced particle migration has been attributed by some researchers as a probable important mechanism for enhanced heat transfer in nanofluids. Particle migration modifies profiles of velocity and thermophysical properties by disturbing the particle concentration distribution; this, as a result, can change the heat transfer rate [13]. The concentration distribution resulting from particle migration depends considerably on parameters such as the mean particle concentration, the size of the particles, Péclet number, and Reynolds number [13]. This results in better heat absorption properties of the base fluid which has been experimentally

tested according to the ASHRAE Standards. The use of nanofluid has a dramatic improvement in the liquid thermo physical properties such as thermal conductivity [14]. Studies have proved the enhancement in thermal conductivity with the dispersion of nanoparticles [15], intensification of turbulence [16], Brownian motion [17], and thermophoresis [18]. Nanoparticles also offer the potential to improve the radiative properties of liquids, leading to enhanced efficiency of the DASCs [19].

The DASC has no resistance between the source and the absorber leading to minimal losses and an improved overall efficiency of the system. According to the results from the study [20], under similar operating conditions, the efficiency of a direct absorption solar receiver (DASR) using nanofluid as the working fluid is found to be up to 10% higher (on an absolute basis) than that of a flat-plate collector. In a proposed method [9] of improving the efficiency of the DASC, 20 nm Al_2O_3 nanoparticle was used with the base fluid (distilled H_2O) in concentrations of 10, 50 and 100 ppm. The DASC showed a respective increase in efficiency by 22.1% for the 10 ppm, and 39.6% for the 50 ppm concentration [9].

An experimental study used carbon-black (0.005 to 0.020 wt.%) nanofluids and a biodegradable fluid (coffee colloid) in a novel pump-free DASC [21]. The results revealed a thermal enhancement of 102% with the carbon black nanoparticle concentration of 0.010 wt. % w.r.t the base fluid. The carbon black nanofluids showed superior results compared to water while the biodegradable fluids showed insignificant improvements. The authors of [22] studied the thermal performance of a DASC (Figure 5) with TiO_2-water as the HTF with various flow rates (2 lpm, 2.5 lpm and 1.5 lpm) with five volume fractions of nanofluids viz. 0.001%, 0.003%, 0.004%, 0.005%, and 0.007%. They concluded that (a) a flow rate of 2.5 lpm showed the best results, (b) with water, the thermal performance at 2 lpm was better, and (c) the nanofluid volume concentration of 0.005% yielded the best results overall.

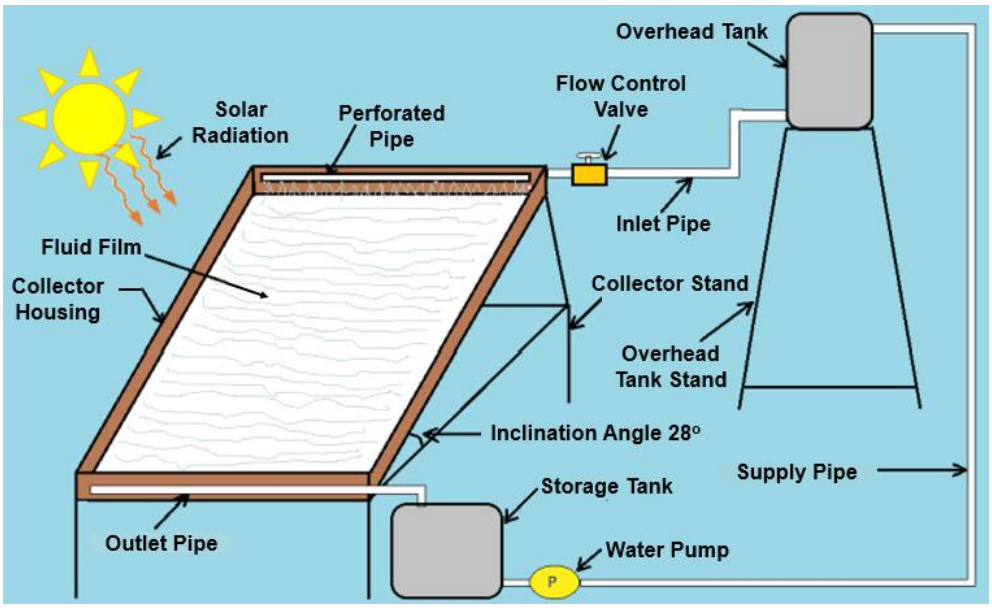

Figure 5. A direct absorption solar collector [22].

The authors [1,23] reported that the efficiency of conventional tube-in plate type solar collectors was limited due to the higher heat losses for surface based solar energy absorption and indirect transfer of heat from hot absorber surface to working fluid having poor heat transfer properties flowing through the tubes. According to an earlier investigation [1], a prototype direct absorption solar collector having gross area of 1.4 m^2 and working on the principle of volumetric absorption was developed to investigate the effect of using Al_2O_3-H_2O nanofluid as the heat transfer fluid with different flow rates. Experiments were carried out using distilled water as base fluid and 0.005% volume fraction of 20 nm Al_2O_3 nanoparticles at a flow rate of 1.5, 2 and 2.5 lpm. ASHRAE 93-1986 (RA 91) [24] standard was followed for the calculation of instantaneous efficiency of the solar collector. Use of nanofluid improves the optical and thermophysical properties that results into an increase in the efficiency of the collector as compared to the use of water alone. An efficiency enhancement of 8.1% and 4.2% was observed in the collector for a flow rate of 1.5 and 2 lpm respectively with the nanofluid than that of

water. The optimum flow rate of 2.5 and 2 lpm was observed for water and nanofluid respectively towards obtaining the maximum collector efficiency. However, in that study, the optimization impact for the different tilt angles was not considered, which is also one of the key contributing factors for the enhancement in efficiency.
In the study presented within this paper, the performance of a DASC was experimentally investigated at different tilt angles to analyse the settling phenomenon of the nanoparticles [25,26] in the base fluid at these angles. The settling of the nanoparticles poses hindrance to the absorption of solar energy and to get the maximum energy absorption [20], an optimum tilt angle plays a crucial role. In DASCs, the tilt is necessary to maintain the flow of fluid in a closed loop because the absorption of energy in nanofluid takes place on a flat glass plate.

Very few studies have evaluated the impact of both tilt angle and the rate of flow of the glass plate simultaneously on the performance of direct absorption solar collectors. In this paper, the performance of a direct absorption solar collector is investigated at different tilt angles of the glass plate (viz. 15°, 20°, and 30°) with respect to the horizontal. The nanofluid flows over the transparent glass plate where the absorption of the solar energy takes place. Also, the impact of different flow rates i.e., 0.5 L/min, 1 L/min and 1.33 L/min on efficiency of DASCs was studied and compared for all the three tilt angles of the glass plate.

The experimental work carried out in this paper is envisaged to help the advancement of solar thermal technologies through research and demonstration to enable improvements in the technical performance of a special case of solar thermal collector (STC) known as Direct Absorption Solar Collector (DASC). This will eventually help lowering the operational costs and reduce the market barriers of emerging solar thermal technologies towards achieving the 2030 deployment milestone.

2. Methodology

2.1. Experimental Set Up

A schematic layout, and the photographs of the experimental set up for the direct absorption solar collector for the study are shown in Figures 6 and 7 respectively. Experimental test setup consists of solar collector, working fluid and data acquisition system. It consists of the top glass cover mounted over a wooden box with insulation on all four inner walls, the base glass plate on which nanofluid flows, the lower tank for collection of nanofluid after getting heated from solar radiation and the header pipe for film type flow. The setup is pictorially represented in Figure 7. A flow rate control valve with the help of a rotameter was used to control the flow rate of the nanofluids over the solar collector. The size of the collector was selected as 600 mm x 600 mm to minimize the overall quantity of nanofluids used [27]. For storing the nanofluids, a 1 litre bottle was selected to get the desired mass flow rate of the nanofluid.

To measure the temperatures, J-type thermocouples were used at both the inlet and the outlet of the flow. The inlet temperature (T1) to the solar collector and the outlet temperature (T2) from the collector were measured using a digital thermometer [28]. For calculating the incoming solar irradiation values, a Pyranometer (Kipp and Zonen) [29] was used and for the calculation of the flow rate, a Rotameter was used. A multichannel digital temperature scanner was employed for temperature measurements, operating within a temperature range of −40 °C to +150 °C and capable of measuring temperatures in environments with irradiation levels up to 4000 W/m^2.

The solar collector was experimentally investigated at the site of the MBM Engineering College, Jodhpur, Rajasthan, India (26.2389° N, 73.0243° E). The collector was oriented due south with varying tilt angles. The experimental tests were performed on the DASC set up from 9 a.m. to 5 p.m. during the month of June. The experiment was repeated on three consecutive days and the average of this was used for assessing the final data. The nanofluid flows over a glass base plate, which is used in place of a black absorber, as is typically used in conventional solar collectors. After the nanofluid is heated in the solar collector, it is then pumped from the lower tank to an upper tank, passing through a heat exchanger. This upper tank could serve as an additional storage or distribution point for the heated fluid. Figure 6 in the circuit diagram consist of flow control valve. This valve is essential for maintaining the required flow rate for the solar collector. The liquid temperature was stabilized by heat exchanger, which is essential for maintaining a constant inlet temperature of the solar collector at 26 °C. This helps in regulating the temperature of the nanofluid entering the collector. Al_2O_3 nanoparticles were mixed in the base fluid (water) to obtain a volume concentration of 0.003%. Adding solid nano Al_2O_3 particles enhanced the thermophysical properties of the heat exchanging medium by improving the

nanofluid heat transfer coefficient and the thermal conductivity, leading to an improved efficiency of the DASC [1,30,31]. The volume concentration in the nanofluid was kept low so that the particle migration in the flow of the fluid enhances the overall heat transfer to the working fluid via convection [32].

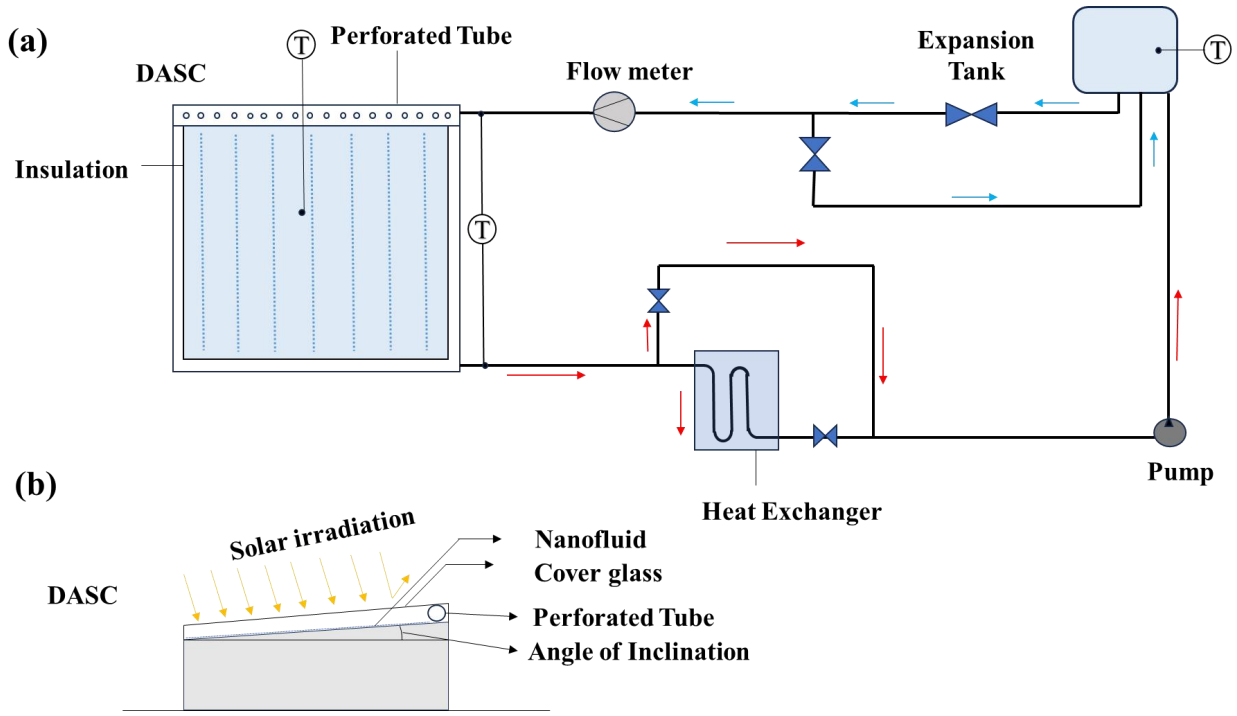

Figure 6. A schematic representation of the experimental setup (**a**) Top view (**b**) Side view.

Figure 7. Pictures of the experimental set up for the direct absorption solar collector.

2.2. Testing Method

The thermal performance of the solar collectors is commonly evaluated using ASHRAE Standard 93-86 which is published by the National Bureau of Standards and is used for testing and rating solar collectors based

on their thermal performances [33]. It is evaluated in terms of instantaneous efficiency, which is dependent on several variables such as the incident solar radiations, the tilt angles, ambient temperatures, the effective specific heat of the nanofluids, global solar irradiation, the area of the absorber plate, and the mass flow rates of the fluids. For the experiments conducted here, the intensity of the incident solar radiations and the useful heat gain by the working fluid at various tilt angles and mass flow rates [24] were measured under steady state conditions. As per ASHRAE Standard 93-86, [24] the steady-state conditions should be maintained during the data period and also during a specified time interval prior to the data period, called the pre-data period. For attaining steady state conditions [12], the mass flow rate must be within ±1%, irradiation must be within ±50 W/m^2, the outdoor ambient temperature must not vary more than ±1.5 K, and the inlet temperature must be within ±0.1 K for the entire test period.

2.3. Instrument Specification

A detailed overview of the various parameters and their corresponding values for the instruments utilized in the experiment are given in Table 1. The instruments include a pyranometer manufactured by Kipp and Zonen, employed for the measurement of solar radiation. Additionally, a simple 8-channel data scanner was utilized in conjunction with J-type thermocouples to measure temperature at various time intervals.

To quantify the flow rate of the nanofluid, a rotameter was installed. Rotameters are devices that measure the flow rate of a fluid by utilizing a tapered tube and a floating indicator. This instrument is particularly useful for determining the flow of nanofluids, where precise control is essential.

One critical aspect of the experimental setup involved ultrasonication, a process conducted for 4–5 hours. Ultrasonication is a technique that employs high-frequency sound waves to agitate particles in a liquid. In this case, it was employed to mix the calculated amount of nanoparticles into the base fluid thoroughly. This step is crucial to prevent the settling of nanoparticles, ensuring a homogeneous distribution within the nanofluid. The use of a sonicator, a device designed for ultrasonication, facilitates the uniform dispersion of nanoparticles, enhancing the overall stability and effectiveness of the nanofluid.

In summary, the experiment involved precise measurements of solar radiation, temperature, and nanofluid flow rate using specialized instruments. The incorporation of ultrasonication was a key step in ensuring the thorough mixing of nanoparticles in the base fluid, contributing to the reliability and accuracy of the experimental results.

Table 1. Description and specification of instruments used in Experimentation.

Parameters	Values
(i) Pyranometer *(Kipp and Zonen, model CM4)*	
Spectral range(50% points)	300 to 2800nm
Sensitivity	4–10 μV/W/m^2
Response time	<8 s
Operational temperature range	−40°C to +150 °C
Maximum solar irradiance	4000 W/m^2
Field view	180°
(ii) Data logger (Make – *Countronics)*	
Accuracy	−50 °C to 750 °C
Range	±1%
(iii) Rotameter (Make – *Flowtech)*	
Accuracy	(/−2% FSD)
Pressure	40 bar
(iv) Ultrasonicator (Make - *Bioera, Model-ULS-01)*	
Operating frequency	−20 to 25 kHz, 950 W
(v) Digital weighing machine (Make - *Ace, Model-KD 200)*	
Least count	0.2 mg

2.4. Nanofluid Preparation

The preparation of a stable nanofluid with a uniform dispersion is an important requirement for improving the heat transfer performance of conventional fluids. The three methods available for the preparation of stable nanofluids are [34].

i. Surfactant addition to the base fluid.
ii. Acid treatment of base fluid.
iii. Ultrasonic mixing of nano powder in base liquid.

Ultrasonication is a better technique for the dispersion of the aggregated particles [35]. In this experiment, the ultrasonication tank was used to prepare nanofluid with enhanced dispersion properties. Nanoparticle Al_2O_3 was purchased from *Reinste Nanoventure Pvt. Ltd.*, Ghaziabad, India, for which the specifications are listed in Table 2.

Table 2. Physical properties of nano particles.

S. No.	Physical properties of Nano particles	Value
1	Sample quantity	10 grams
2	Particle shape	Spherical
3	Average particle size	50 nm
4	Particle size full range	10–140 nm
5	Specific surface area	8 m^2/g
6	Purity of particle	99.75 %

To prepare the Al_2O_3 nanofluid, the mass of Al_2O_3 was calculated using Equations (1) and (2) given below to obtain the desired concentration [36].

$$m_p = V_T \varphi_p \times \rho_p \quad (1)$$

$$V_{nf} = V_P + V_f \quad (2)$$

where:
φ_p = Volume fraction of nanoparticle
ρ_p = Density of the nanoparticles (kg/m^3)
m_p= Mass of the nanoparticle (kg)
V_{nf}= Total volume of the nanofluid (m^3)
V_p= Volume of the particle (m^3)
V_f = Volume of the base fluid (m^3)

The quantity of base fluid (water) V_f = 3000 mL
Density of Al_2O_3 particles ρ_p = 3.9 g/cm^3
Density of water, ρ_f = 1000 kg/m^3

The Al_2O_3 nanofluid with distilled water as the base fluid was ultrasonicated in the vibration tank for 4–5 hours and then left to settle the nanoparticle at the bottom of the flask for more than 24 hours. During the experiment, the time taken to perform the runs was kept below the first settlement to get efficient dispersion of the nanoparticles in the base fluid [37].

2.5. Solar Collector Performance: Governing Equations

The instantaneous efficiency was calculated and compared for the different tilt angles and mass flow rates using Equation (3) [38]. Other parameters are calculated using Equations (4)–(7). ASHRAE Standards were referred to, while calculating the efficiency to ensure accuracy in the results. Specifications for the solar collector are given in Table 3, and the data on the average solar irradiance at the experimental site for the months of January to July are shown in Table 4.

$$\text{Collector efficiency, } \eta = \dot{m}\, C_{nf}\, (T_{out} - T_{in})/IA \quad (3)$$

$$\text{Mass flow rate, } \dot{m} = \rho_{nf} \times A \times v \quad (4)$$

$$\text{Effective density of Nanofluid, } \rho_{nf} = (1 - \varphi_p)\rho_f + \varphi_p \rho_p \quad (5)$$

$$\text{Volume fraction, } \varphi_p = V_p/(V_p + V_f) \quad (6)$$

$$\text{Specific heat, } C_{nf} = \left[(1 - \varphi_p)\rho_f\, c_f + \varphi_p \rho_p c_p\right]/\rho_{nf} \quad (7)$$

where η = Instantaneous efficiency (%)
$\dot{m}$ = Mass flow rate of the working fluid (L/min)
C_{nf} = Effective specific heat of the Nanofluids $\left(\frac{kJ}{kg}/°C\right)$
T_{out} = Outlet temperature of the working fluid (°C)
T_{in} = Inlet temperature of the working fluid (°C)
I = Global solar irradiation (W/m^2)
A = Area of the absorber plate (m^2)
ρ_{nf} = Density of the Nanofluids (kg/m^3)
v = velocity of the fluid (m/s)
φ_p = Volume fraction of the nanoparticles
ρ_f = Density of the nanofluids (kg/m^3)
ρ_p = Density of the nanoparticles (kg/m^3)
V_P = Volume of the nanoparticles (m^3)
V_f = Volume of the base fluid (m^3)

Table 3. Specifications of the solar collector.

Component	Dimensions	Material
Collector size	600 mm x 600 mm	Wood
Glass plate	620 mm x 600 mm	Toughened glass
Header pipe	550 mm (Length)	Plastic
Inner insulation	10 mm thick	Thermocol/Styrofoam

Table 4. Average solar insolation per day for the months of January to July in the test location (Jodhpur, India).

Month	Average Solar Insolation (kWh/m^2)
January	4.07
February	4.95
March	6.12
April	6.77
May	6.83
June	6.66
July	5.63

2.6. Experimental Errors

As per the ASME [39] guidelines, errors arise due to various reasons and absolute measurement of these errors is very difficult while taking readings. Data acquisition errors, calibration errors and data reduction errors are some of the major errors involved during experimentation while measuring flow rate, temperature, and solar radiation intensity. Table 5 highlights the quantitative uncertainty in the various parameters relevant to this analysis calculated using Equation (8).

Table 5. Uncertainty analysis of the parameters.

S. No	Parameter	Uncertainty
1	Volumetric flow	±2%
2	Solar Intensity	±5.5%
3	Temperature difference	±2%

General form of equation for uncertainty analysis is as given below:

$$U_y{}^2 = \sum_{i=1}^{n} U_{Xi}^2 \tag{8}$$

Where, U_y is the total uncertainty of the calculated parameter and U_{Xi}^2 is root square uncertainty of each parameter.

The combined uncertainty for calculating the collector efficiency, U_η was obtained by Root Sum Square method (RSS) as given by the relation in Equation (9):

$$(U_\eta)^2 = [(\nabla \dot{m}/\dot{m})^2 + (\nabla(T_{out} - T_{in})/(T_{out} - T_{in}))^2 + (\nabla I/I)^2 \tag{9}$$

The uncertainty in this experimental study was calculated as 6% using the above formulae while conducting various tests for determining the collector efficiency.

3. Results

3.1. Effects of Varying Mass Flow Rates for a Given Tilt Angle

The experimental efficiency for the DASC at the different tilt angles for the various flow rates is graphically represented in Figures 8 – 10 respectively.

3.1.1. Tilt Angle 15°; Mass Flow Rate Varied from 0.5, 1 and 1.5 L/min

The experiment was conducted keeping the tilt angle of the glass plate at 15° using nanofluids for the DASC. The experiments started at 9 a.m. till the stagnation point was reached for 0.5 L/min flow rate. Similarly, the readings were taken for 1 L/min and 1.33 L/min keeping the tilt angle constant at 15°. For this experiment, the inlet temperature was kept constant at 26 °C using a heat exchanger. The results are graphically plotted as shown in Figure 8.

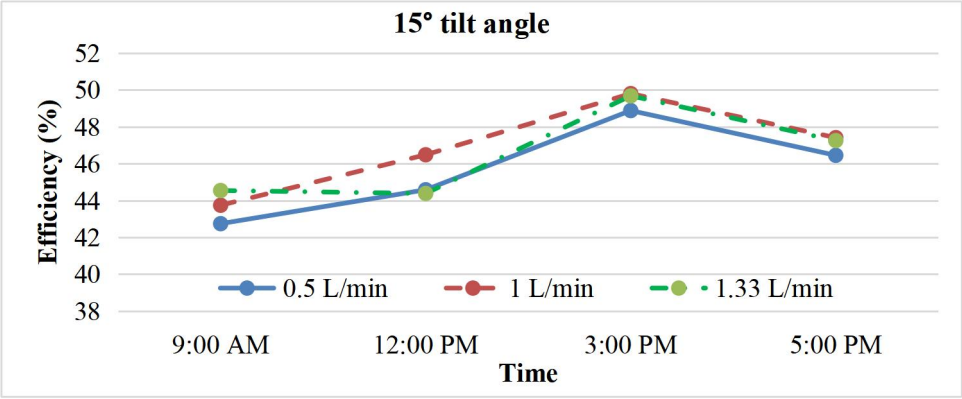

Figure 8. The efficiency of the solar collector (%) versus the time of the day for different mass flow rates (L/min) at a tilt angle of 15°.

3.1.2. Tilt Angle 20°; Mass Flow Rate Varied from 0.5, 1 and 1.33 L/min

When the tilt angle of the glass plate was increased to 20° for the flow rates of 0.5 L/min, 1 L/min and 1.33 L/min, the results obtained are graphically plotted in Figure 9.

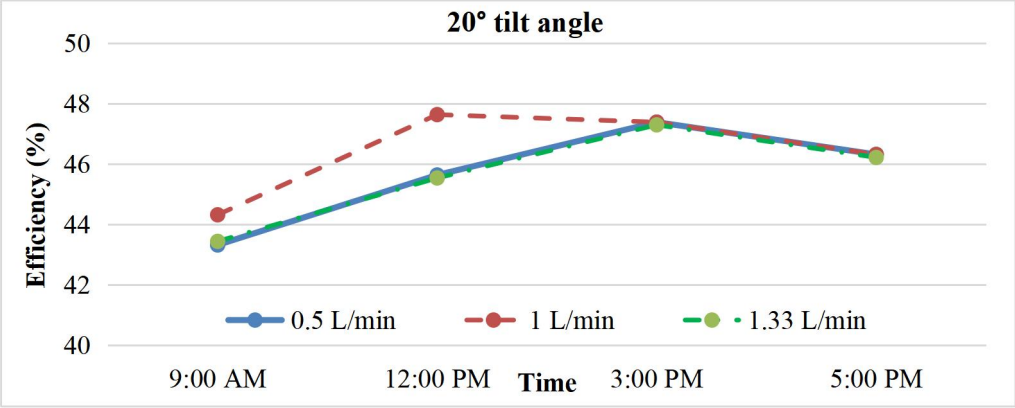

Figure 9. The efficiency of the solar collector (%) versus the time of the day for different mass flow rates (L/min) at a tilt angle of 20°.

3.1.3. Tilt Angle 30°; Mass Flow Rate Varied from 0.5, 1 and 1.33 L/min

The tilt angle of the glass plate was increased further to 30° with the nanofluids. The experiment was done at the mass flow rates of 0.5 L/min, 1 L/min, and 1.33 L/min respectively starting at 9 a.m. The results are graphically plotted in Figure 10.

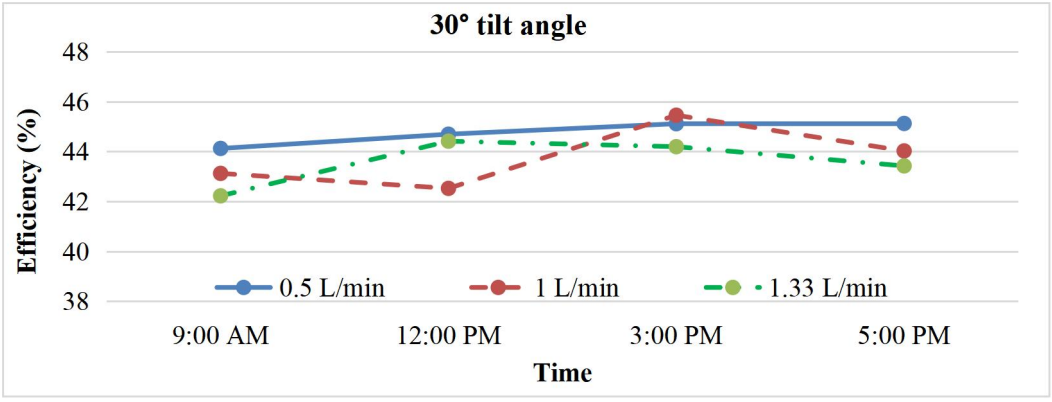

Figure 10. The efficiency of the solar collector (percentage) versus the time of the day for different mass flow rates (L/min) at a tilt angle of 30°.

3.2. Impact of Change in Parameters over the DASC System Efficiency

The consolidated results from the experiments, showing the calculated efficiencies of the DASC at a specific time with respect to the tilt angles, are shown in Figure 11a. Similarly, the efficiencies concerning various flow rates are presented in Figure 11b.

4. Discussions

To study the effects of various parameters on the performance of a direct absorption solar collector (DASC), a series of experiments were conducted in India (26.2389°N, 73.0243°E) for three different tilt angles of 15°, 20°, and 30° using Al_2O_3-H_2O nanofluids. Mass flow rates of 0.5 L/min, 1 L/min, and 1.33 L/min were used for the three different tilt angles. The experimental setup was under observation from 9 a.m. until 5 p.m. on three separate days and average data is presented in the final results. Since the experiment was conducted over consecutive clear sky days in the month of June, an almost similar measured solar radiation of 6.66 kWh/m^2 was noticed throughout the experimentation. The average temperature variation during June was recorded with a minimum value of 29 °C and a maximum value of 39 °C. Similarly, the hourly variations from 9 a.m. to 5 p.m. stayed within 27 °C and 35 °C. The maximum temperature difference between the inlet and outlet temperatures of the collector was recorded at a lower tilt angle, i.e., 15°. This phenomenon was attributed to the prolonged residence time of the fluid on the glass base plate at this angle. Similarly, as the tilt angle increased, the

temperature difference between the inlet and outlet of the solar collector also decreased. The efficiencies of the solar collector for different tilt angles, and mass flow rates are calculated using Equation (3).

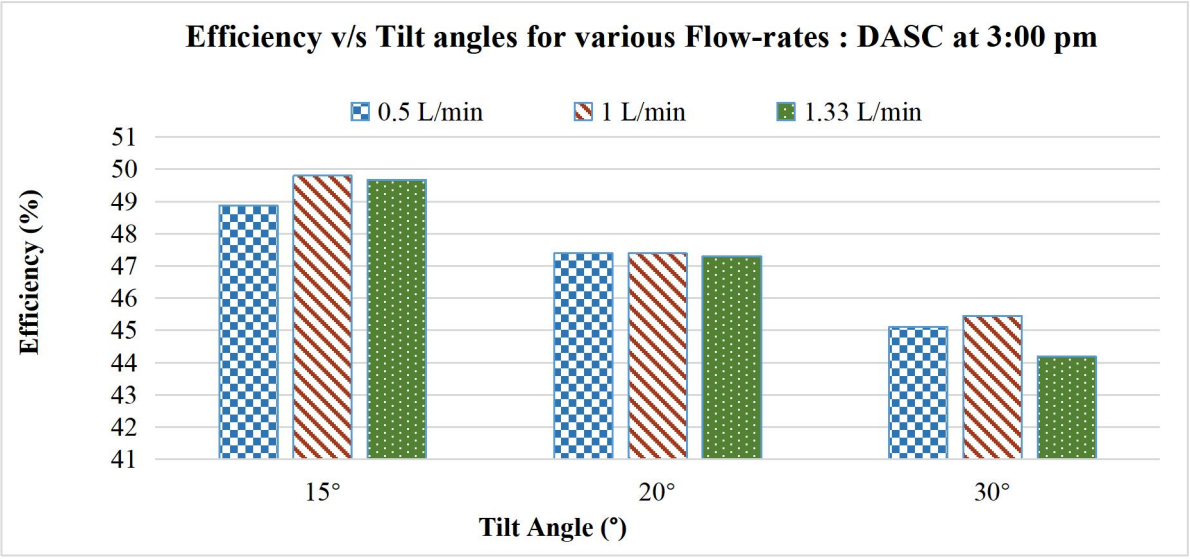

(a)

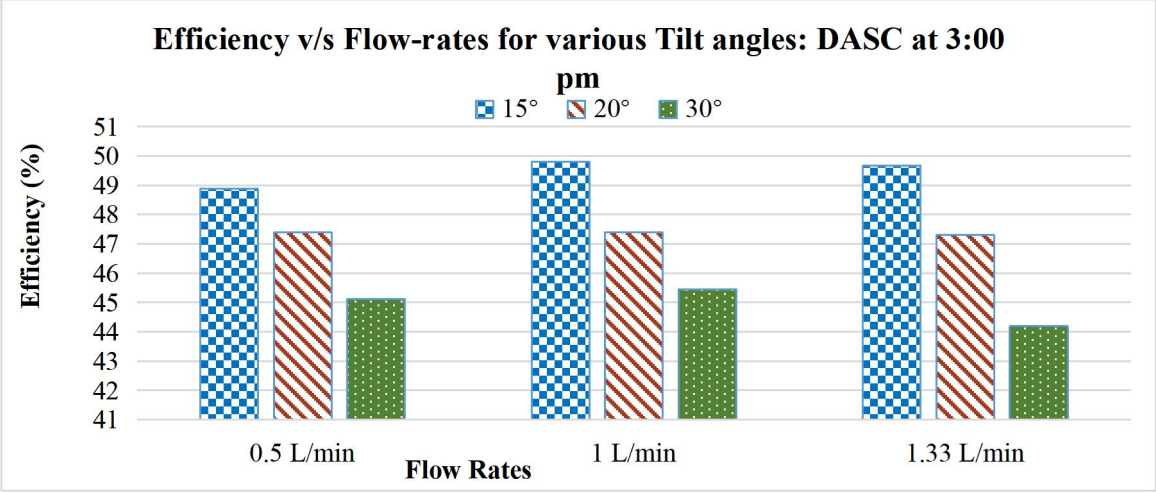

(b)

Figure 11. Consolidated results from the experiments on DASC: calculated system efficiency (%) at 3 p.m. with respect to the: (**a**) three tilt angles for the various flow-rates, and (**b**) three flow-rates at various tit angles.

It can be observed that for a tilt angle of 15° and the same flow rates, the efficiency of the collector initially increases till 3 p.m. and then starts to decrease. This is due to the fact that the sun goes overhead during forenoon while sun rays are slanting during morning and evening. It is observed that as the flow rate increases from 0.5 L/min to 1 L/min, the efficiency increases but it slightly reduces for 1.33 L/min compared to 1 L/min flow rate. The optimum flow rate for maximum efficiency was 1 L/min in this study.

Similarly, for a tilt angle of 20° the efficiency increases till 3 p.m. and then starts to show a decline due to the slanting of the sunlight, and with an increase in the flow rate from 0.5 to 1 L/min, the efficiency increases except for a slight reduction at 1.33 L/min. It was also observed that for a tilt angle of 20° the initial efficiency was higher compared to a tilt angle of 15°. According to Planck's law, the emissive power is proportional to the fourth power of its absolute temperature and at higher temperature of the working fluid, increased emissive losses take place resulting in lower collector efficiency. Thus, at a 20° angle, as the radiation losses increase compared to 15°, it results in a lower efficiency later in the day.

For a tilt angle of 30° during the morning and afternoon time, the efficiency was lesser due to slanted rays. It can be seen that as the tilt angle was increased to 30°, the gain in efficiency due to the increased flow rate was not appreciable.

At a higher tilt angle, the time for fluid residence was lesser due to the higher velocity of the fluid which leads to a reduced heat transfer. It was observed that the overall efficiency was highest for a 15° tilt angle at a flow rate of 1 L/min. The maximum efficiency was observed at 3 p.m. within the whole day, w.r.t the flow rates for the various tilt angles.

As can be seen, a 15° tilt angle gives the best efficiencies for all three mass flow rates of 0.5, 1 and 1.33 L/min followed by 20° and 30° respectively. In essence, an increase in the tilt angle reduces the efficiency of the DASC system.

The flow rate of 1 L/min seems optimum for the tilt angles of both 15°, 20° and 30°. As the flow rate increases over 1 L/min, the residence period of the nanofluid within the system reduces which results in lower heat transfer to the working fluid. Also, the maximum solar insolation is absorbed for lower tilt angles, since increasing the tilt angle reduces the incident irradiance. At a lower tilt angle, the fluid residence time over the plate increases, leading to higher heat absorption and an initial rise in efficiency. It is evident from this experimental study that an optimum flow rate and tilt angle must be maintained to obtain the maximum solar efficiency. As seen in the literature, this study also supports that there is an optimum flow rate for a specific nanofluid where efficiency is maximized. This combination of tilt angle with flow rate of nanofluid in the DASC system is an improvement over the previous study.

5. Future Perspectives

In the future, it is recommended that similar studies be conducted at the same location with the same setup for different seasons to ascertain the effect of weather conditions. In addition, more detailed experimental analysis with similar setups with the incorporation of the other novel nanofluids could enhance the performance of the DASC. This could enhance the future STC technologies substantially through incremental technological improvements. This research paves the way for meeting the ever-increasing targets for worldwide solar thermal installations as advocated by the IEA Net Zero Emissions by 2050 Scenario. It directly aligns with the UN SDG 7 (access to affordable, reliable, sustainable, and modern energy), SDG 9 (resilient infrastructure, sustainable industrialization and foster innovation) and SDG 11 (safe, resilient and sustainable cities and human settlements).

6. Conclusions

The following key conclusions can be drawn from this study with respect to (a) the tilt angle of the solar collector, and (b) the mass flow rate of the nanofluid over the collector surface:

(i) The overall efficiency of the DASC reduces at higher tilt angles compared to the lower tilt angles for all three mass flow rates. The data on the average efficiencies calculated over a whole day showed that a 15° tilt angle shows the best results for 0.5, 1 and 1.33 L/min (45.66, 46.86, 46.71% respectively) followed by 20° (45.67, 46.42, 45.07%) and 30° (44.76, 43.78, 43.56%) respectively. Therefore, a tilt angle of 15° could be selected as the optimum.

(ii) The general trend for the DASC system showed that an increase in the tilt angle reduces the overall system efficiency by 2.44% and 4.35% respectively for a flow rate of 1 L/min.

(iii) At a flow rate of 1 L/min, the maximum efficiency was achieved for the tilt angles of 15°, 20° and 30° (49.80, 47.39 and 45.45% respectively) at 3 p.m. where maximum efficiencies were achieved for the DASC. Hence, 1 L/min could be considered the optimum mass flow rate.

It can be concluded that the optimum tilt angle must be maintained in a DASC while the fluid flows over the glass plate. The parameters such as film energy absorption, and the flow rate must also be optimum to obtain the maximum efficiency.

Nomenclature

A	Solar Collector or absorber plate Area (m^2)
C_p	Specific Heat capacity of the working fluid (J/kg·K)
C_r	Correction Factor
I	Solar Irradiation (W/m^2)
k	Thermal Conductivity of the working fluid (W/m·K)
m	Mass of the fluid (kg)
$\dot{m}$	Mass flow rate of the working fluid (L/min)
n	Shape factor
Q_a	Heat absorbed by the solar collector (W)
Q_i	Total Average Solar Radiation fall on the collector (W/m^2)
T	Temperature of the working fluid (K)
U_y	Total uncertainty
U_η	Combined uncertainty
V	Volume of the fluid (m^3)
W	Weight of the fluid ($kg·m/s^2$)

Greek Symbols

φ	% of Volume Fraction
η	Collector Efficiency
ρ	Density (kg/m^3)

Subscripts

f	Base Fluid
nf	Nano Fluid
p	Nanoparticle
in	Initial Condition
out	Final Condition

References

1. Gupta, H.K.; Agrawal, G.D.; Mathur, J. Investigations for effect of Al_2O_3–H_2O nanofluid flow rate on the efficiency of direct absorption solar collector. *Case Stud. Therm. Eng.* **2015**, *5*, 70–78. [CrossRef]
2. Rai, G.D. *Solar energy utilisation*, 5th ed.; Khanna Publishers: New Delhi, India, 1995.
3. Sukhatme, S. *Solar energy fundamental and applications*; Tata Mcgraw Hill Publication: New York, US, 1984.
4. Taylor, R.A.; Phelan, P.E.; Otanicar, T.P.; Walker, C.A.; Nguyen, M.; Trimble, S.; Prasher, R. Applicability of nanofluids in high flux solar collectors. *J. Renew. Sustain. Ener.* **2011**, *3*, 023104. [CrossRef]
5. Solar Heat Worldwide: Global Market Development and Trends 2021. Available online: https://www.iea-shc.org/Data/Sites/1/publications/Solar-Heat-Worldwide-2022.pdf.
6. IEA. Solar thermal technologies deployed in around 400 million dwellings by 2030. In *Technology and innovation pathways for zero-carbon-ready buildings by 2030*; IEA: Paris, French, 2022.
7. Mousavi Ajarostaghi, S.S.; Mousavi, S.S. Solar energy conversion technologies: principles and advancements. In *Solar energy advancements in agriculture and food production systems;* Gorjian, S.; Campana, P.E. Eds.; Academic Press: Cambridge, UK, 2022. pp. 29–76.[CrossRef]
8. Selvakumar, N.; Barshilia, H.C.; Rajam, K.S. Review of sputter deposited mid-to high-temperature solar selective coatings for flat plate/evacuated tube collectors and solar thermal power generation applications. *NAL Project Document SE*. **2010**.
9. Gupta, H.K.; Agarwal, G.D.; Mathur, J. Experimental evaluation on the effect of nanofluids concentration on the performance of Direct absorption solar collector. *Int. J. Adv. Eng. Nanotechnol.* **2014**, *1*(12), 16–20.
10. Sainz-Mañas, M.; Bataille, F.; Caliot, C.; Vossier, A.; Flamant, G. Direct absorption nanofluid-based solar collectors for low and medium temperatures. A review. *Energy.* **2022**, *260*, 124916. [CrossRef]

11. Otanicar, T.P.; Phelan, P.E.; Golden, J.S. Optical properties of liquids for direct absorption solar thermal energy systems. *Sol. Energy.* **2009**, *83*, 969–977. [CrossRef]
12. Minardi, J.E.; Chuang, H.N. Performance of a "black" liquid flat-plate solar collector. *Sol. Energy.* **1975**, *17*, 179–183. [CrossRef]
13. Bahiraei, M. Particle migration in nanofluids: A critical review. *Int. J. Therm. Sci.* **2016**, *109*, 90–113. [CrossRef]
14. Peyghambarzadeh, S.M.; Hashemabadi, S.H.; Naraki, M.; Vermahmoudi, A. Experimental study of overall heat transfer coefficient in the application of dilute nanofluids in the car radiator. *Appl. Therm. Eng.* **2013**, *52*, 8–16. [CrossRef]
15. Wang, X.Q.; Mujumdar, A.S. Heat transfer characteristics of nanofluids: A review. *Int. J. Therm. Sci.* **2007**, *46*, 1–19. [CrossRef]
16. Pak, B.C.; Cho, Y.I. Hydrodynamic and heat transfer study of dispersed fluids with submicron metallic oxide particles. *Exp. Heat Transf.* **1998**, *11*, 151–170. [CrossRef]
17. Xuan, Y.; Li, Q. Heat transfer enhancement of nanofluids. *Int. J. Heat Fluid Flow.* **2000**, *21*, 58–64. [CrossRef]
18. Koo, J.; Kleinstreuer, C. Impact analysis of nanoparticle motion mechanisms on the thermal conductivity of nanofluids. *Int. Commun. Heat Mass Transf.* **2005**, *32*, 1111–1118. [CrossRef]
19. Mu, L.; Zhu, Q.; Si, L. Radiative properties of nanofluids and performance of a direct solar absorber using nanofluids. In Proceedings of the ASME 2009 Second International Conference on Micro/Nanoscale Heat and Mass Transfer, Shanghai, China, 18–21 December 2009. [CrossRef]
20. Tyagi, H.; Phelan, P.; Prasher, R. Predicted efficiency of a low-temperature nanofluid-based direct absorption solar collector. *J. Sol. Energy Eng.* **2009**, *131*, 041004. [CrossRef]
21. Trong Tam, N.; Viet Phuong, N.; Hong Khoi, P.; Ngoc Minh, P.; Afrand, M.; Van Trinh, P.; Thang, B.H.; Żyła, G.; Estellé, P. Carbon nanomaterial-based nanofluids for direct thermal solar absorption. *Nanomater.* **2020**, *10*, 1199. [CrossRef]
22. Khatri, R.; Kumar, M.; Jiyani, R. An experimental investigation on direct absorption solar collector using TiO_2-water nanofluid. In Proceedings of the 2018 2nd International Conference on Green Energy and Applications (ICGEA), Singapore, 24–26 March 2018. [CrossRef]
23. Otanicar, T.P.; Phelan, P.E.; Prasher, R.S.; Rosengarten, G.; Taylor, R.A. Nanofluid-based direct absorption solar collector. *J. Renew. Sustain. Ener.* **2010**, *2*, 033102. [CrossRef]
24. Huang, B.J.; Hsieh, S.W. An automation of collector testing and modification of ANSI/ASHRAE 93-1986 standard. *J. Sol. Energy Eng.* **1990**, *112*, 257–267. [CrossRef]
25. Timofeeva, E.V.; Yu, W.; France, D.M.; Singh, D.; Routbort, J.L. Nanofluids for heat transfer: An engineering approach. *Nanoscale. Res. Lett.* **2011**, *6*, 182. [CrossRef]
26. Khanafer, K.; Vafai, K. A critical synthesis of thermophysical characteristics of nanofluids. In *Nanotechnology and energy*; Jenny Stanford Publishing: Dubai, U.A.E., 2017; pp. 279–332.
27. Han, Z. Nanofluids with enhanced thermal transport properties. Ph.D. thesis, University of Maryland at College Park, College Park, Maryland, 2008.
28. Best Practices Handbook for the Collection and Use of Solar Resource Data for Solar Energy Applications. Available online: https://www.nrel.gov/docs/fy21osti/77635.pdf.
29. Zonen, K., *CMP11 Pyranomètre*, in *CMP11 Pyranomètre*, O.H. B.V., Editor. 2021, https://www.kippzonen.com/Product/114/CMP11-Pyranometre. OTT HydroMet B.V.: The Netherlands.
30. Ajeeb, W.; da Silva, R.R.T.; Murshed, S.S. Experimental investigation of heat transfer performance of Al_2O_3 nanofluids in a compact plate heat exchanger. *Appl. Therm. Eng.* **2023**, *218*, 119321. [CrossRef]
31. Rashmi, W.; Ismail, A.F.; Asrar, W.; Khalid, M.; Faridah, Y. Natural convection heat transfer in nanofluids: A numerical study. In Proceedings of the ASME 2008 Fluids Engineering Division Summer Meeting, Jacksonville, Florida, USA, 10–14 August 2008.
32. Bahiraei, M.; Hosseinalipour, S.M. Particle migration in nanofluids considering thermophoresis and its effect on convective heat transfer. *Thermochim. Acta.* **2013**, *574*, 47–54. [CrossRef]
33. Mumma, S.A.; Yellott, J.I.; Wood, B. Application of ASHRAE standard 93-77 to the thermal performance testing of air solar collectors. *ASHRAE J.* **1978**, *84*.
34. Trisaksri, V.; Wongwises, S. Critical review of heat transfer characteristics of nanofluids. Available online: https://www.osti.gov/biblio/6149565.
35. Mahbubul, I.M.; Saidur, R.; Amalina, M.A.; Elcioglu, E.B.; Okutucu-Ozyurt, T. Effective ultrasonication process for better colloidal dispersion of nanofluid. *Ultrason. Sonochem.* **2015**, *26*, 361–369. [CrossRef]
36. Gupta, H.K.; Agrawal, G.D.; Mathur, J. An overview of Nanofluids: A new media towards green environment. *Int. J. Environ. Sci.* **2012**, *3*, 433–440. [CrossRef]
37. Choudhary, R.; Khurana, D.; Kumar, A.; Subudhi, S. Stability analysis of Al_2O_3/water nanofluids. *J. Exp. Nanosci.* **2017**, *12*, 140–151. [CrossRef]
38. Behura, A.K.; Gupta, H.K. Efficient direct absorption solar collector using Nanomaterial suspended heat transfer fluid. *Mater. Today Proc.* **2020**, *22*, 1664–1668. [CrossRef]

39. Lee, S.; Choi, S.S.; Li, S.A.; Eastman, J.A. Measuring thermal conductivity of fluids containing oxide nanoparticles. *J. Heat Transfer* **1999**, *121*, 280–289. [CrossRef]